Chapter 12

Study of Composite and Sandwich Plates Extracted from Wind Turbine Blade Structures under Harsh Environmental Conditions

Bong Taek Oh

Mechanical Design Engineering, ChungNam National University/Adjunct Professor
CEO, TOMS Co., LTD. /Center for Composite Materials
296-3 Seonjin-li Sachun-si Gyeonsangnam-do Rm.317 Seoul, Korea
btoh@tomskorea.kr

I. INTRODUCTION

For current reliability and safety standards, the efficiency of a wind turbine plant depends mainly on the capacity of the rotor blades to extract energy from the incoming wind. Because of strong competition from other energy sources, wind turbines must be cost-effective. In determining their cost, material selection and manufacturing processes are crucial. Modern wind turbine blades are constructed with fiber-reinforced plastics (FRP) owing to their superior strength-to-weight ratio. Most wind turbines, both large and small, have the same basic parts: blades, shafts, gears, generator, and a cable. These components work together to convert the wind energy into electricity. As we know wind turbines detain the most energy using the propeller-like blades. So the blades are the most important parts of a wind turbine. The cost to manufacture a wind turbine blade is about 15–20% of the turbine's total production cost. In order to increase their energy conversion efficiency, the size of blades have becomes larger, blade diameters ranging from 20 to 100 meters or more [1]. However, these lager blades are encountering harsher and more complex service environments, which have led to several safety problems. The blades can be damaged by moisture absorption, sleet, ultraviolet radiation, atmospheric corrosion, fatigue, wind gusts, or lightning strikes, to name a few hazards. Wind turbine blade failure is very costly because it can damage other blades, the turbine itself, and other turbines located in neighborhood [1]. Clearly, it is important to detect any damage before it leads to catastrophic blade failure.

II. TRANSIENT THERMAL STRESS ANALYSIS OF LAMINATED COMPOSITE

Because wind speed generally increases by 0.1m/s per 100m of altitude for the first 1000m, high altitudes are often the best sites for wind farms. However, wind farms located at high altitudes in cold regions often face icing conditions during the winter. Icing happens when supercooled water droplets hit a surface colder than 0 ℃ and freeze upon impact. To understand the behaviour of wind turbine blades under these conditions, transient analysis for composite structure under low temperature is needed [2-3].

A. Transient Thermal Analysis Model

Transient thermal stress analysis was performed using finite element analysis to analyze the thermal stress distribution of a cryogenic composite immersed in liquid nitrogen (LN_2, -196 °C). The representative volume elements and configuration of cryogenic composite are shown in Fig. 1(a) and (b). Fig. 1(a) shows the global and material coordinate systems of composite laminate. The x-y-z axis will designate the global coordinate of a composite piece. Each layer in that composite may have different fiber orientation that will require a separate coordinate system. The direction along the fiber is designated by 1-direction while the direction transverse to it is designated by 2-direction or the matrix direction. The x-y-z and 1-2-3 coordinate systems coincide in the case of uniaxial composite [4].

The temperature distribution can be obtained by solving the transient heat transfer equation for each material point in the laminate for each ply. Eq. (1) can be obtained by considering the uncoupled theory (neglecting the effect of linear thermal expansion coefficient) and no internal heat generation in the heat equation [5].

$$\rho c_p \frac{\partial T}{\partial t} - k_{ij} T_{,ji} = 0 \qquad \text{where } i, j = x, y, z \tag{1}$$

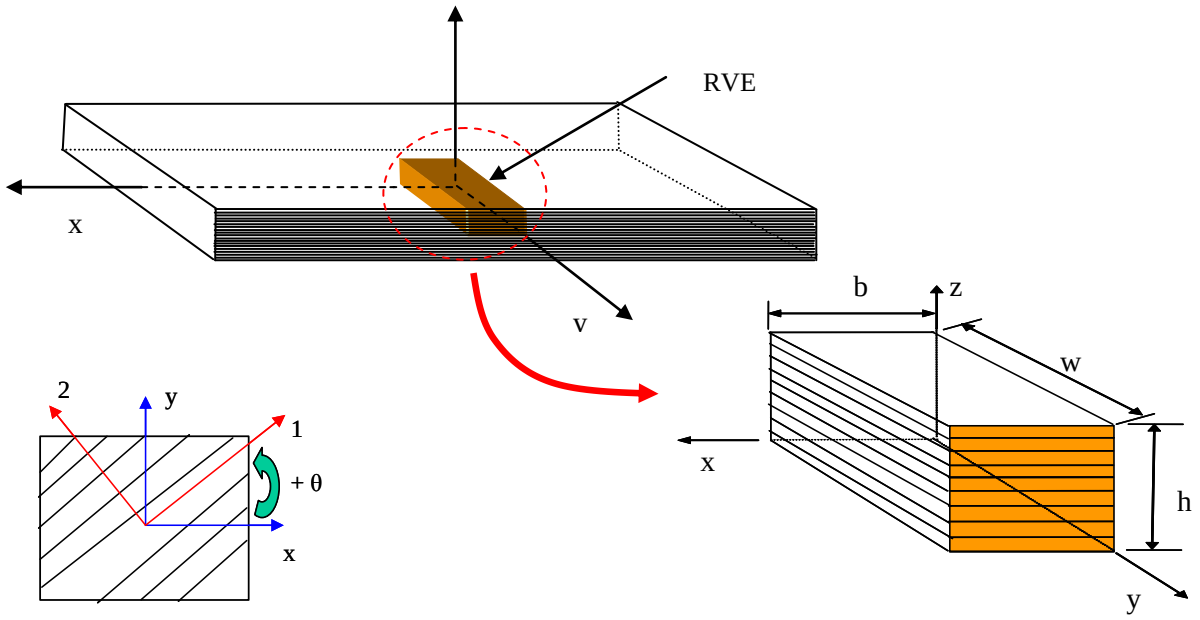

(a) Representative volume element (b) Specimen configuration

Fig. 1 Representative volume element and configuration of a symmetric composite laminate

where k_{ij}, T, ρ and C_p are second-order thermal conductivity tensor, temperature, density and specific heat, respectively. The planes $x = 0$, $x = b$, $y = 0$ and $z = 0$ are assumed to be fully insulated:

$$\frac{\partial T}{\partial n} = 0 \qquad \text{at } x = 0,\ x = b,\ y = 0,\ \text{and } z = 0 \tag{2}$$

where n is the unit normal vector to the respective plane.

The planes $y = w$ and $z = h$ are maintained at -196 °C, that is:

$$T(x, w, z) = T(x, y, h) = -196°C \tag{3}$$

Based on the temperature distribution at every time step of the analysis, the static stress can be calculated using the balance of linear momentum. The dynamic effects are neglected since the time scale is much smaller than the characteristic time for transient heat transfer.

$$\sigma_{ij,j} = 0 \qquad \text{where } i, j = x, y, z \tag{4}$$

where σ_{ij} is the second-order stress tensor. The one-way coupling with the thermal field enters through the constitutive equation for a linear thermoelastic solid:

$$\sigma_{ij} = C_{ijmn}\{\varepsilon_{mn} - \alpha_{mn}\Delta T\} \qquad \text{where } i, j, m, n = x, y, z \tag{5}$$

where $\varepsilon_{mn} = \frac{1}{2}(u_{i,j} + u_{j,i})$; C_{ijmn}, α_{mn}, and u_i are fourth-order elastic stiffness tensor, second-order thermal expansion coefficient tensor, and displacement vector, respectively. Substituting Eq. (5) into Eq. (4), one obtains the following field equation:

$$C_{ijmn}\, u_{m,nj} = C_{ijmn}\, \alpha_{mn}\, T_{,j} \qquad \text{where } i, j, m, n = x, y, z \tag{6}$$

Because of symmetries in the geometric domain shown in Fig. 2, only half of the total numbers of plies were modeled through the thickness, also half of width was modeled through the x-direction. The boundary conditions on the plane $y = 0$ and $z = 0$ can be expressed as follows

$$u_y(x, 0, z) = 0,\ u_z(x, y, 0) = 0 \tag{7}$$

where u_x and u_z are the displacement in the x and z directions, respectively. Due to the periodicity in the *y*-direction, periodic boundary conditions were applied on the planes $x = 0$ and $x = b$ as follows:

$$u_x(0, y, z) = u_x(b, y, z) + < \frac{\partial u_x}{\partial x} > b$$
$$u_y(0, y, z) = u_y(b, y, z) + < \frac{\partial u_y}{\partial x} > b \quad (8)$$
$$u_z(0, y, z) = u_z(b, y, z) + < \frac{\partial u_z}{\partial x} > b$$

where u_x, u_y, and u_z are the displacements in the x, y, and z directions, respectively. The volume averaged displacement gradients, $< \frac{\partial u_x}{\partial x} >$, $< \frac{\partial u_y}{\partial x} >$, and $< \frac{\partial u_z}{\partial x} >$, were treated as unknowns in the finite element analysis, and determined while solving. The planes $y = w$ and $z = h$ have zero traction boundary conditions.

B. Effect of Laminate Thickness

To study the effect of total laminate thickness, symmetric laminates with stacking sequences $[0/-45/90/45/0/45/90/-45/0]_s$ and $[0/-45/90/45/0]_s$ have been adapted for transient analysis of IM7/977-2. As it can be seen from Figs. 2 and 3 that the thicker laminate has higher stress pattern than thinner laminate has.

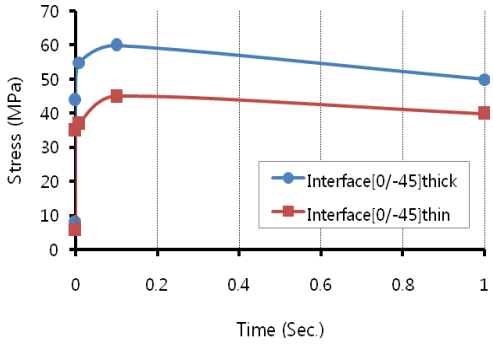

Fig. 2 Out-of-plane stress on surface ply under thermal loading for a $[0/-45/90/45/0/45/90/-45/0]_s$ and $[0/-45/90/45/0]_s$ laminates of IM7/977-2 as a function of time

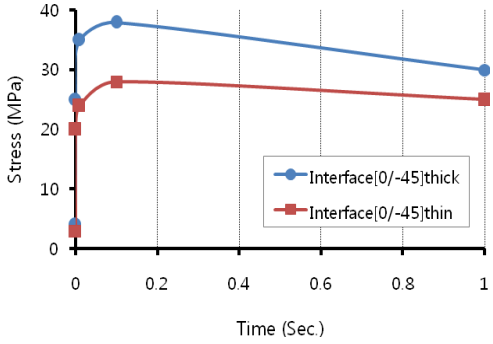

Fig. 3 Out-of-plane stress on surface ply under thermal loading for a $[0/-45/90/45/0/45/90/-45/0]_s$ with 250 μm and 125 μm ply thickness of IM7/5250-4 as a function of time

C. Effect of Ply Thickness

The effect of ply thickness on the free-edge under thermal loading as a function of time was inspected. The thicker ply has higher in-plane stress σ_{22} at the peak point in the stress curve in a very short time. Even higher ply level stress at the peak point in the stress curve was observed for out-of-plane stress σ_{33}, which may cause the delamination on the free-edge. The ply with 250 μm thickness has twice higher out-of-plane stress in a very short time than the ply with 62.5 μm thickness. To reduce the effect of thermal shock, which may cause the delamination, the high peak point stress should be suppressed. The methodology for suppressing the free-edge delamination was investigated in the next section.

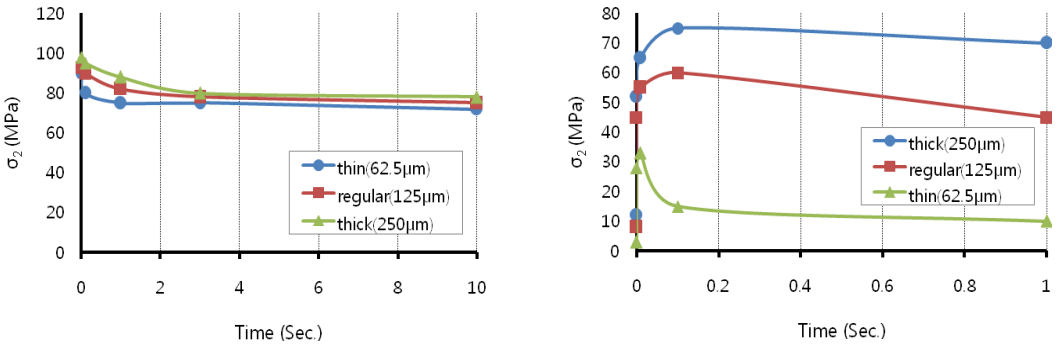

(a) In-plane stress (b) Out-of-plane stress

Fig. 4 Effect of ply thickness on the free-edge under thermal loading for a $[0/-45/90/45/0/45/90/-45/0]_s$ of an IM7/977-2 laminate as a function of time

D. Effect of Insulation Layer

A further investigation of the sudden exposure to cryogenic temperatures was conducted numerically. A lay-up, $[90_2/0_2]_S$, of IM7/5250-4 with and without insulating layer was used for the study of insulation layer on thermal shock. The transient thermomechanical analysis with and without insulation layer was performed using FEA model. In order to reduce the thermal shock, an insulating layer was added to the surface of IM7/5250-4 composite laminate with $[90_2/0_2]_S$. The thermal conductivity of the insulating layer was taken to be about 3 times less than the thermal transverse conductivity of the IM7/5250-4 laminate. Fig. 5 shows the out-of-plane stress distributions without insulation after 0.1, 1, and 20 seconds. Stress distributions with insulation layer after 0.1, 1, 120, and 1800 seconds are shown in Fig. 6. Thickness of the insulating layer was 3mm. Ply level stresses in the laminate without the insulation decreased and saturated after 20 seconds. However, the stresses in the laminate with the insulation increased and saturated after 1800 seconds. Both with and without insulation cases converged to 10 MPa of maximum stress σ_{33} in 90 °ply (Ply 2) as expected.

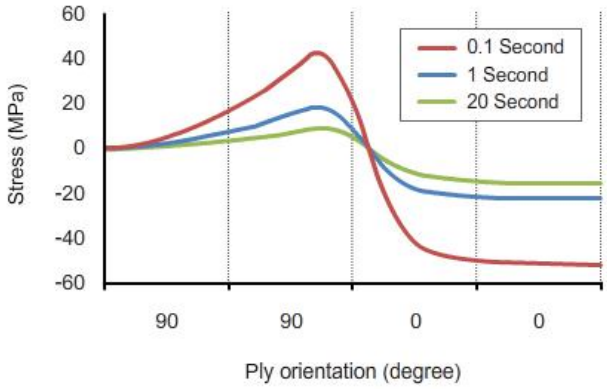

Fig. 5 Stress σ_{33} distributions under thermal loading after 0.1; 1 and 20 seconds without insulation for a $[90_2/0_2]_S$ of an IM7/5250-4 composite laminate

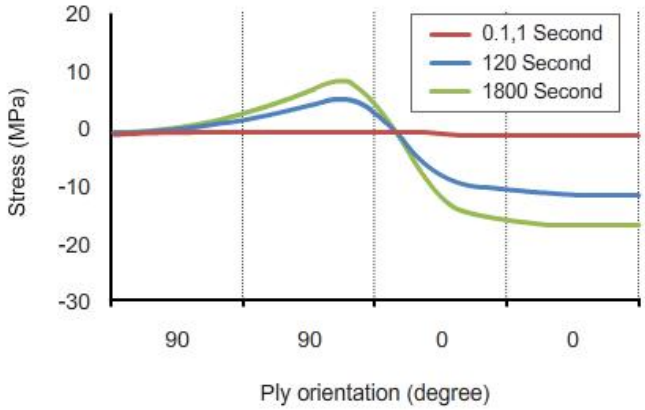

Fig. 6 Stress σ_{33} distributions under thermal loading after 0.1; 1; 120 and 1800 seconds with insulation (3mm) for a $[90_2/0_2]s$ of an IM7/5250-4 composite laminate.

A plot of the maximum value of σ_{33} in 90 °ply (ply 2) as a function of time is shown in Fig. 7 to identify the effect of time and insulation layer.

The peak point in the stress curve (Fig. 7a) was observed for the model without insulation in a very short time. Maximum stress σ_{33} without insulation goes up to 40 MPa, which is 4 times higher than saturated maximum stress (10 MPa), in a very short time. However, there is no peak point in the stress curve for the model with insulation layer (Fig. 7b). The maximum stress in the z-direction, σ_{33}, increased gradually. The peak point in stress curve for the model without insulating layer may have caused edge delaminations in cryogenic composite laminates. Hence, ply-level stress σ_{33} on the free-edges due to thermal shock can be reduced by introducing the insulation layer. Experimental work is needed to compare and verify numerical results for the effect of thermal shock in cryogenic composite laminates. Future study will be focused on the damage characterization on the edge of cryogenic composite laminates with and without insulation layer.

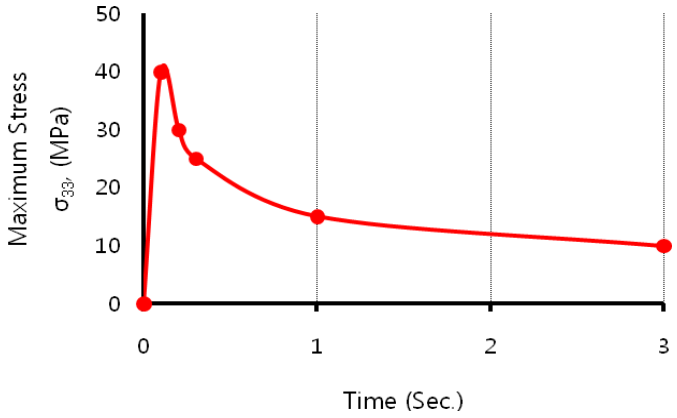

(a) without insulation

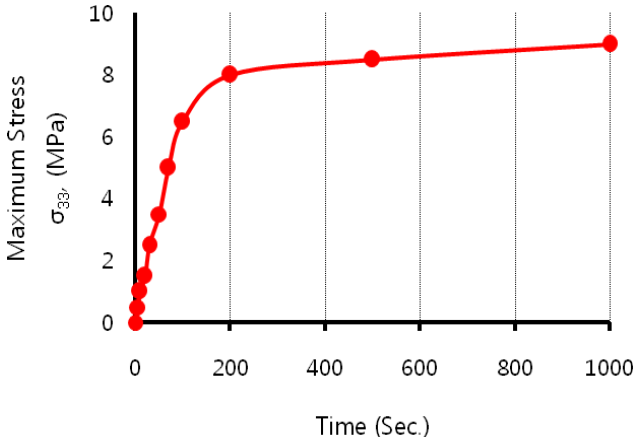

(b) with insulation

Fig. 7 Maximum stresses σ_{33} on 90 °ply as a function of time of an IM7/5250-4 composite laminate

III. DAMAGE CHARACTERIZATION IN COMPOSITES FOR WIND TURBINE BLADES UNDER HARSH ENVIRONMENT

A. Experimental Apparatus and Materials

Pictures of the thermomechanical test system for thermal cycling, uniaxial tension and four-point bending test are shown in Fig. 8(a)-(c), respectively. A high density polyethylene cryogenic dewar shown in Fig. 8(a) was used for the thermal cycles and an MTS 880 Materials Test System was used for the mechanical loading of the composite laminates tested at both room and cryogenic temperatures. Fig. 8(b) shows the custom designed cryogenic chamber for uniaxial tension test, which was mounted on the MTS 880 frame. Since steel has a relatively low thermal conductivity at cryogenic temperatures, the chamber was built of stainless steel. An aluminum foil insulator was added around the chamber in order to improve insulation. A four-point bending test fixture, as shown in Fig. 8(c), for cryogenic environment was developed for small specimens (15 cm in length, 2.54 cm in width). This test was designed to facilitate the study of damage development under variable stress states as is often the case in cryogenic tanks and permeability experiments under load.

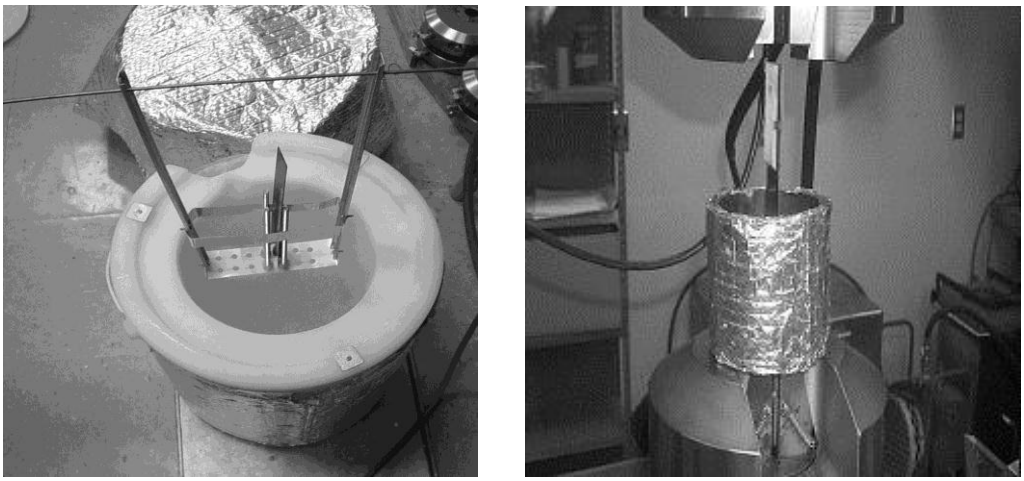

(a) (b)

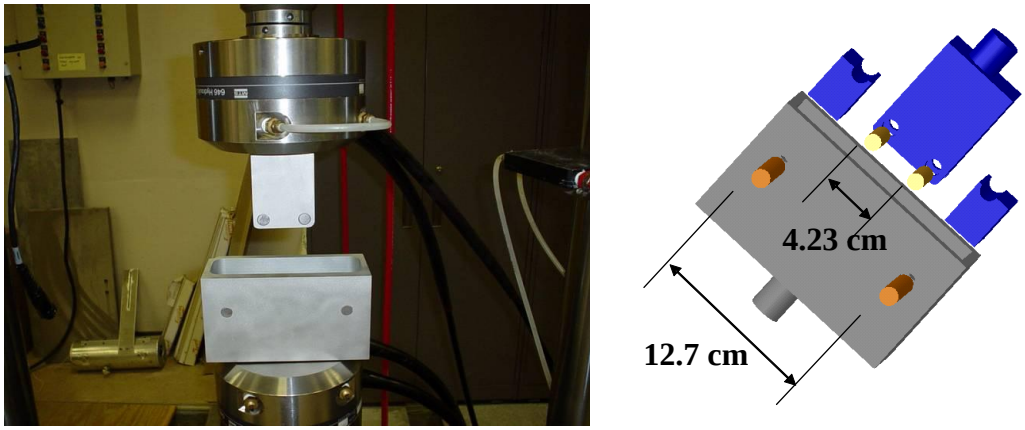

(c)

Fig. 8 Experimental apparatus: (a) cryogenic dewar, (b) cryostat system mounted on an MTS 880 frame and (c) four-point bending test apparatus.

The specimens for both uniaxial tension and four-point bending test were provided by Lockheed Martin and Air Force Research Laboratory (AFRL), respectively. The specimens for uniaxial tension test as shown in Fig. 9(a) were 18-ply graphite epoxy IM7/977-2 laminates with $[0/-45/90/45/0/-45/90/45/0]_S$ stacking sequence, and with dimensions of 15.24 cm [6”] (gage length) x 9.144 cm [3.6”] (width) x 0.225 cm [0.088”] (thickness). The specimens had undergone prior thermomechanical testing, including thermal cycles from room temperature to liquid nitrogen (-196°C) and mechanical cycles at cryogenic temperatures (-196°C). From the specimens received, they were tested under additional thermomechanical loading. For the thermomechanical loading tests, the original specimens were cut into three pieces (A, B and C), as illustrated in Fig. 9(a). The specimens for four-point bending test and thermal shock test as shown in Figs. 9(b) and (c) were 8-ply graphite epoxy IM7/5250-4 laminates with $[90_2/0_2]_S$ stacking sequence. Thermomechanical effective properties for both material systems were found in the literature [6-8].

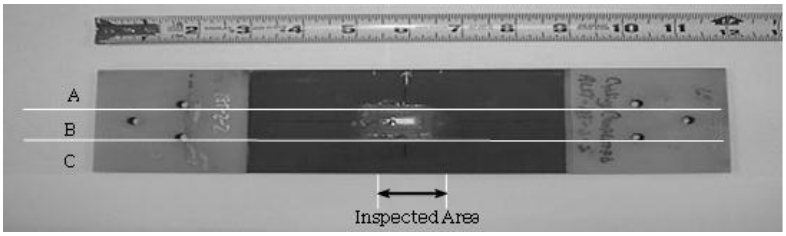

(a)

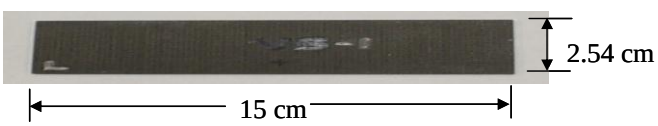

(b)

(c)

Fig. 9 Cryogenic composite laminates: (a) IM7/977-2, (b) IM7/5250-4, (c) IM7/5250-4 without insulation (left) and with insulation (right).

B. Thermomechanical Cycles

Thermal loading usually consists of cycling between room or a higher temperature and a cryogenic temperature (most often liquid nitrogen, i.e. –196°C). Mechanical loading typically takes place at cryogenic temperatures, with an applied maximum stress level being a portion of the ultimate strength. Combined thermal cyclic loading (room temperature to -196°C) and mechanical loading at -196°C and room temperature are performed on cryogenic composite laminates for the uniaxial tension test. More specifically, thermal cycling (room temperature to -196°C) in the absence of mechanical load, thermal cycling followed by mechanical cycling at room temperature, and mechanical cycling at cryogenic temperatures as well as mechanical loading at room temperature are the loading paths that have been investigated as shown in Fig. 10 for 18-ply graphite epoxy IM7/977-2 laminates with $[0/-45/90/45/0/-45/90/45/0]_S$ stacking sequence. First, a laminate specimen was mechanically tested at room temperature in uniaxial tension to failure in order to determine the Young's modulus and ultimate tensile strength.

During the mechanical loading, the stress and strain values were obtained. The strain values were calculated by using the cross-head displacement, while the stress values were determined from a load cell attached on the cross-head. The Young's modulus and ultimate tensile strength were determined to be 61.2 GPa and 787.02 MPa, respectively. Then, a second laminate was cut into three pieces from the original specimen shown in Fig. 9(a), and machined with a dimension of 25.4 cm x 2.54 cm (10" x 1") according to ASTM standards, D3039/3039M-00 recommendation. Three specimens were tested with three loading paths as shown in Fig. 3.

IM7/5250-4 laminates with $[90_2/0_2]_S$ stacking sequence was cycled using four-point bending test system. The first and second specimens underwent four-point bending test at room temperature (RT), and the third specimen was subjected four-point bending test at -196 ℃. However, higher bending moment was applied to the second specimen at RT. A bending moment of 0.573 $N{\cdot}m$ was applied to first and third specimens, which results to a maximum tensile stress equal to 40% of the ultimate tensile strength on the outer 90 ° ply. For the second specimen, a bending moment of 1.21 $N{\cdot}m$ was applied so that the maximum tensile stress on the 90 ° ply is the same with the maximum tensile stress used by a combined mechanical and thermal loading.

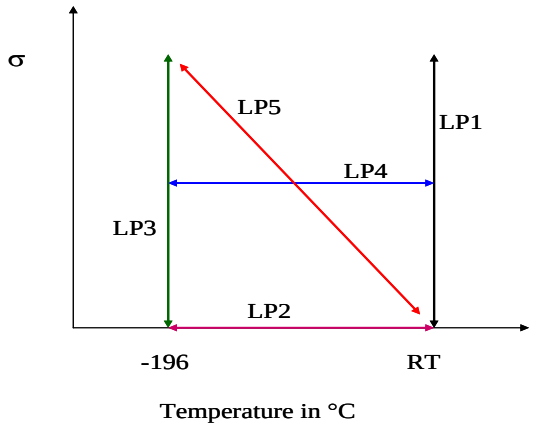

Fig. 10 Various thermomechanical loading paths

C. Damage Analysis (Microcrack Density)

In this section, the experimental work on characterization of damage developed during thermomechanical cycling of cryogenic composite laminates will be discussed. Some researchers [9-12] have studied the damage evolution of cryogenic composites by applying different types of thermomechanical loading. This section is focused on damage analysis of cryogenic composite laminates subjected to thermomechanical load. The attention is given to the local multiaxial stress field (along the fibers direction) which is generated in the material and that is due to the orthotropic behavior. In composite materials, especially under fatigue loading, the presence of a multiple cracking condition is common; for this reason in order to evaluate the damage evolution it is very useful to consider the crack density as controlling parameter. In this section, only the transverse matrix crack was counted for crack density. The crack density is parameterized by summing over all plies the number of cracks in each ply per unit length on free-edge.

The three specimens for uniaxial tension test, indicated as A, B, and C in Fig. 9(a), were characterized for damage before any loading cycle was applied. Cracks were counted in each non-zero degree ply along a 32 mm (1.26") span centered lengthwise on each specimen. Specimen A underwent a total of 20 thermal cycles. Specimen B was subjected to two thermal cycles followed by two mechanical cycles at 60% of the ultimate tensile strength at room temperature. The four cycles were repeated three times, and the specimen was inspected after each mechanical and thermal loading cycle. Mechanical loading at cryogenic temperatures was applied to specimen C. More specifically, specimen C was immersed for 30 minutes in liquid nitrogen to guarantee that it had reached the same temperature as liquid nitrogen. Subsequently, the specimen was mechanically loaded while still being held in the liquid nitrogen, but the test was terminated early due to delamination reaching the grips. The specimen was examined using an optical microscope to collect damage state information, such as crack density for each ply and delamination length occurring at interfaces between plies. Fig. 11 shows the crack densities of the second ply from the outer surface [-45 °], and their increase with the number of loading cycles for specimens A, B, and C, respectively.

Similar trend in the rate of crack density growth has been observed in the third ply [90 °] of the specimens tested. The zero in the horizontal axis describes the initial state of each specimen, while each cycle on the graph corresponds to two physical cycles, either mechanical or thermal. When thermal cycles (specimen A) alone were applied, there were no additional cracks in the material up to 20 cycles. However, thermal cycling, followed by mechanical cycling at room temperature (specimen B), resulted in a rapid increase of microcracking induced damage, which saturated after it reached a level of about eight times the initial damage. Even higher rate of increase of damage densities was observed in specimen C, which was mechanically cycled at cryogenic temperatures, but delamination at the grips resulted in termination of the experiment.

The three specimens for four-point bending test, indicated as LP-A, B, and C in Fig. 12, were characterized for damage before any loading cycle was applied. Cracks were counted in each 90 degree ply along a 25.4 mm (1.0") span centered lengthwise on each specimen. Specimen LP-A underwent a total of 840 four-point bending test at room temperature. Specimen LP-B was subjected to higher bending moment at room temperature. The bending moment was applied to specimen LP-C at cryogenic temperature. The damage information was collected using the optical microscope for every 5 cycle.

Fig. 12 shows the crack density on the first ply from the outer 90 °ply, and their increase with the number of loading cycles for mechanical loadings at RT and -196 ℃, respectively. No cracking occurred up to 500 cycles for four-point bending test with the bending moment of 0.573 N·m at RT. However, four-point bending test at -196 ℃ resulted in TMC after 10 cycles. Higher bending moment was applied to verify if the cracks resulted due to the difference of ply level stress. After 10 cycles, the second specimen had almost the same crack densities with four-point bending test at -196 ℃. However it had about half the crack density after 30 cycles. The brittle nature of the specimen under cryogenic temperatures could be the cause for this difference. Results presented in [13-14] show the influence of cryogenic service temperatures on the strength, modulus, and fracture of IM7/977-3, a toughened graphite/epoxy. It was reported that the material becomes very brittle and the strength and modulus change at cryogenic temperature.

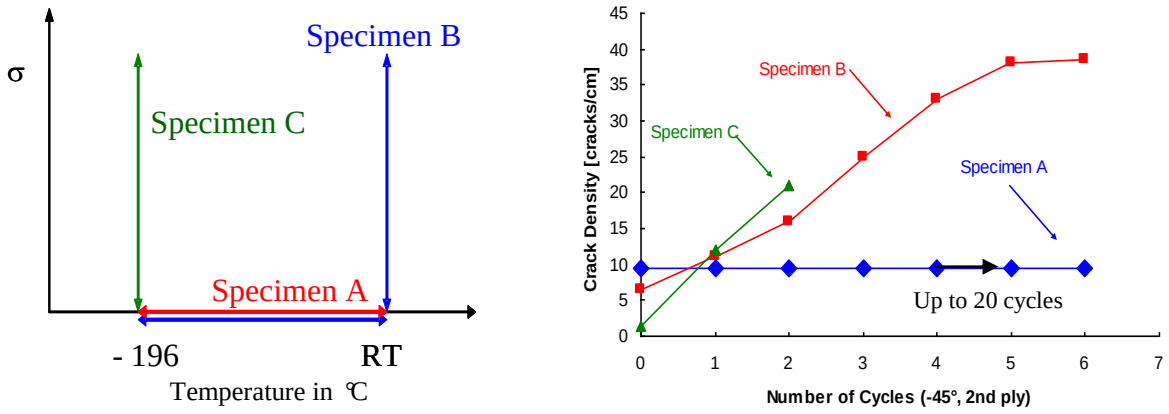

Fig. 11 Micro-crack density versus number of cycles for the [–45 °] ply (second from outer surface) of IM7/977-2 laminates with $[0/-45/90/45/0/-45/90/45/0]_S$ under uniaxial tension loading

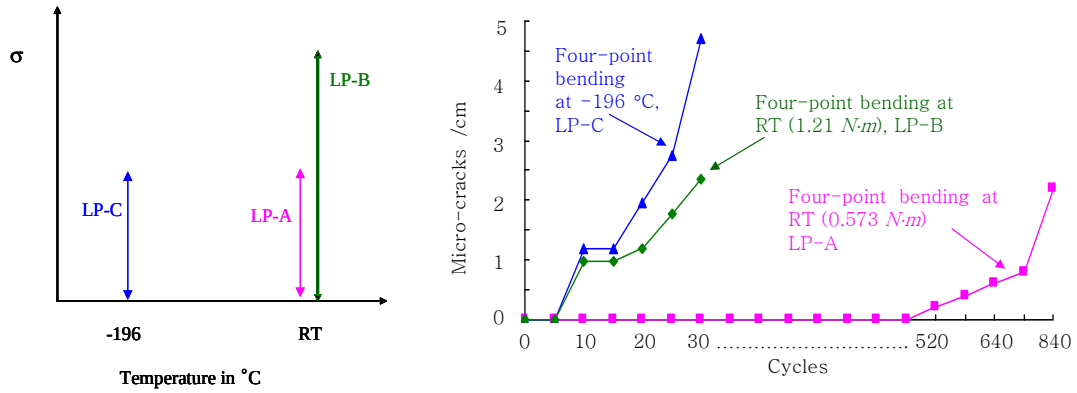

Fig. 12 Micro-crack density versus number of cycles for the [90 ¶ ply of IM7/5250-4 laminates with $[90_2/0_2]_S$ under four-point bending

Fig. 13 shows typical optical micrographs taken in the middle of the specimen edge at the end of the loading cycles. The initial damage state, which is the damage of specimen A, is shown in Fig. 13(a). The damage state after twelve loading cycles for specimen B and four mechanical cycles at cryogenic temperature for specimen C are shown in Figs. 13(b) and 13(c), respectively. Cracks were found only in plies 2, 3, and 4 in the $[0/-45/90/45/0/-45/90/45/0]_S$ laminate. No cracks were found in plies 15, 16 and 17. This is an unusual case (considering symmetric lay-up of the laminate) and a possible cause can be due to the presence of residual stresses resulting from manufacturing process or stress concentrations at micro cracks in the plies 2, 3 and 4. Delaminations were observed between plies 2-3, and 3-4. The majority of the interface cracks were observed between plies 2-3, as shown in Fig. 13(c).

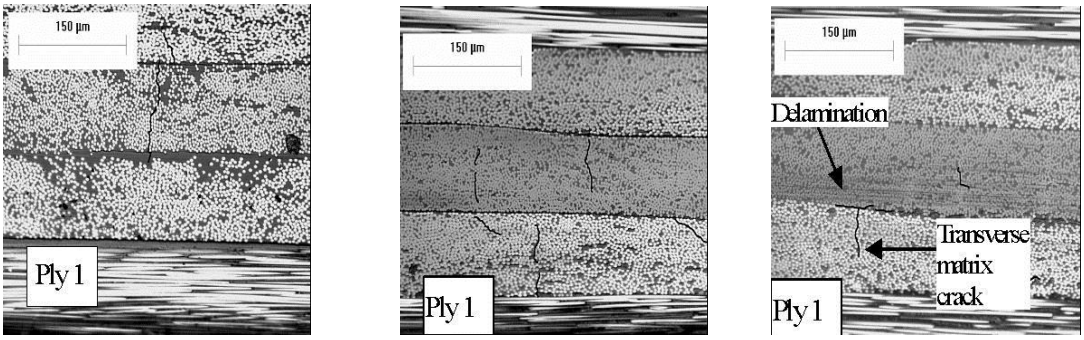

(a) (b) (c)

Fig. 13 Micrographs showing damage under uniaxial tension test: (a) specimen A, (b) specimen B, and (c) specimen C

From the above results, one can conclude that for simultaneous mechanical loading in a cryogenic environment, the chances of delamination and hence leakage is higher than thermal testing followed by mechanical loading at room temperature. Delaminations at transverse crack tips were also observed, which could be more critical for the permeability and leakage problem.

Figs. 14 and 15 show the optical micrographs for the four-point bending tests conducted under different loading paths. The initial state (damage free state), is shown in Fig. 14(a). The damage states after 50 and 520 loading cycles are shown in Fig. 14(b) and 14(c), respectively. Under cryogenic testing, the damage states before and after 10 loading cycles are shown in Fig. 15(a) and 15(b), respectively.

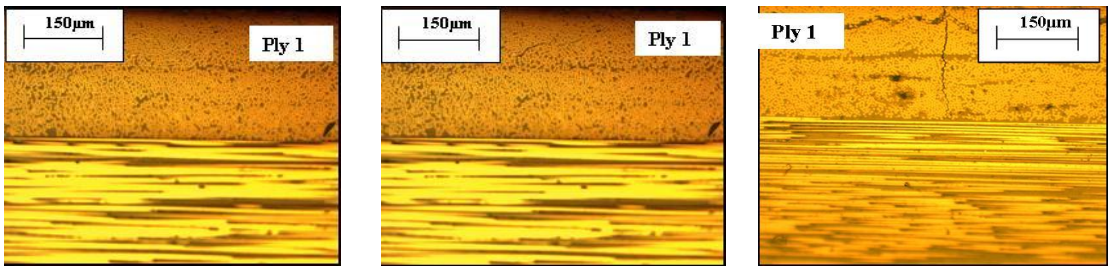

(a) (b) (c)

Fig. 14 Micrographs showing damage under four-point bending test at room temperature:
(a) before testing, (b) after 50 cycles, and (c) after 520 cycles

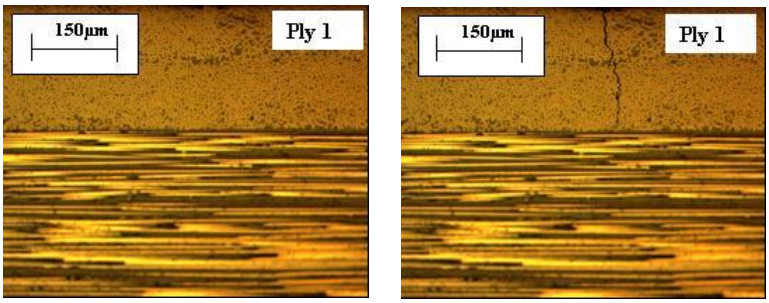

(a) (b)

Fig. 15 Micrographs showing damage under four-point bending test at -196 ℃: (a) before testing and (b) after 10 cycles

After thermomechanical loading cycles, delaminations were observed along the interface on the free-edges. The sudden exposure to cryogenic temperatures may have caused the delaminations and transverse matrix crack (TMC) on the free-edges, due to large temperature variation through the thickness and the resulting thermal stresses. Fig. 16 shows the experimental set-up and surface temperature results for wax insulation. Paraffin wax was used as an insulation material under cryogenic environment. A thermocouple was placed between wax and specimen surface. The surface of the specimen reaches LN2 temperature immediately without insulation, but with 3.5mm paraffin wax insulation it took 60 seconds to reach near LN2 temperature, which substantially reduces the thermal gradient in the laminate.

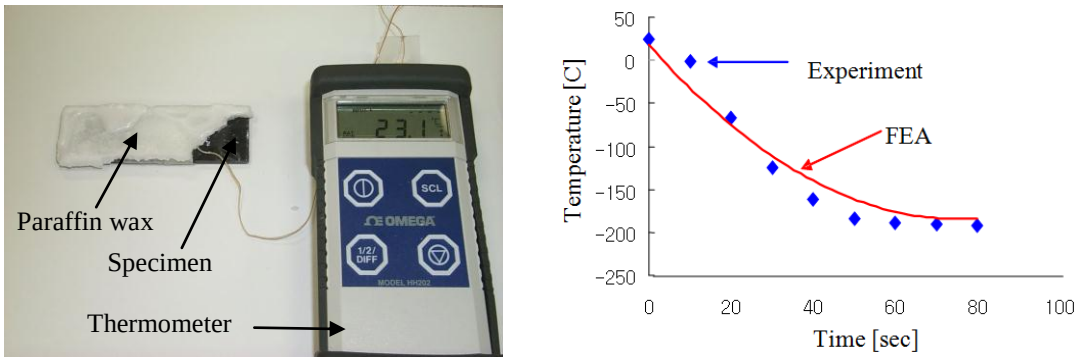

Fig. 16 Experimental set-up and surface temperature result for wax insulation

Thermal cycling was experimentally performed to verify the effect of thermal shock on damage in cryogenic composite laminates. The specimens tested were provided by AFRL, and they were 8-ply graphite epoxy IM7/5250-4 laminates with $[90_2/0_2]_S$ stacking sequence. The two specimens were characterized for the damage state before any loading cycle was applied. The TMC were counted in each 90 degree ply along a 30 mm span centered lengthwise on each specimen. The first specimen without wax insulation underwent a total of 45 thermal cycles, and characterized after every thermal cycle. The second specimen with wax insulation was subjected to a total of 40 thermal cycles. Fig. 17 shows the transverse crack densities of the 90 degree ply, and their increase with the number of loading cycles for the first and second specimens, respectively. When thermal cycles were applied to the second specimen, there were no TMC on the free-edges for 40 cycles. However, the TMC were initiated for the first specimen after 33 thermal cycles. Therefore, TMC observed in the first specimen are from thermal shock but not from thermal cycles. It is possible to remove the thermal shock effect on the edge during cryogenic test using wax insulation.

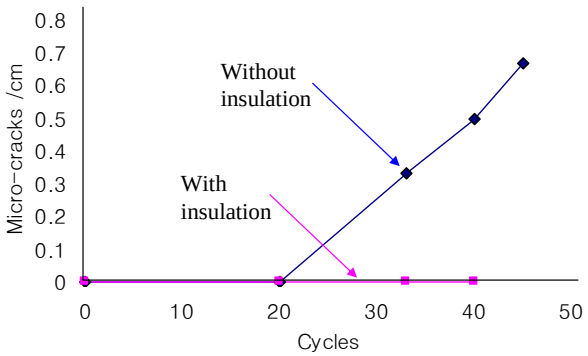

Fig. 17 Crack density vs. number of thermal cycles without and with wax

IV. PREDICTION OF MICROCRACKING

A. *Building RVE (Representative Volume Element) using FE Model*

Most of the analytical work for formation of damage was on transverse matrix cracks. However, initial studies were conducted and are continuing to determine the interaction of transverse matrix cracks and delaminations

In order to simulate cracks occurring in laminates a finite element model for a representative volume element (RVE) was built. The RVE (or unit cell) is defined herein as the smallest region that represents the behavior of the entire region without any mirroring or rotation transformations. Fig. 18(a) shows a laminate with matrix cracks, which are idealized based on the assumptions that the cracks are parallel to the *x1x3*-plane and extend through the entire length and thickness of the ply. The cracks are also assumed to be periodically distributed. Due to the assumptions, periodic boundary conditions are applied to the RVE. The RVE with one crack is extracted from the laminate. A finite element mesh was built for this RVE as shown in Fig. 18(b). The degree of degradation of a cracked laminate is directly related to the crack opening displacements.

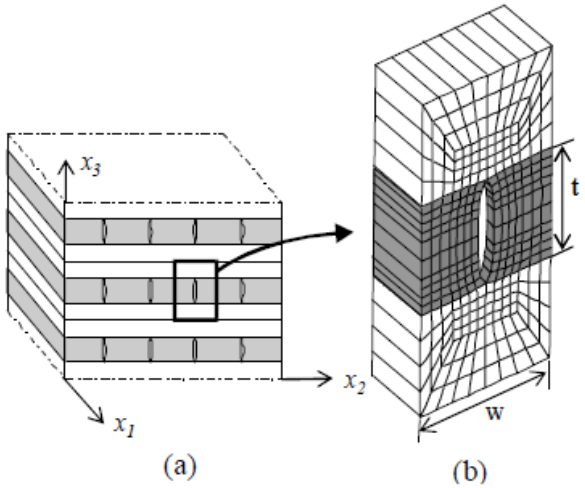

Fig. 18 Modeling a laminate with transeverse matrix cracks (TMC)

B. *Calculating COV (Crack Opening Volume) for a Laminate*

Since the damage level will increase with crack opening volume (COV), it is essential that we understand crack opening and factors that affect the crack opening. One of objectives in the current work is to show that the crack opening volume can be directly related to the degradation behavior of the effective moduli of a cracked ply. A simple expression for the COV will be derived based on the modulus reduction and the volume averaged strain or stress of a cracked ply for a given crack density. The study on the opening will extend to consider the delamination and matrix cracking together.

C. *Modeling of Delamination at the Intersection of Cracks*

Microcracking can lead to other forms of damage such as delamination. Laminate design may have a significant effect on the delamination initiation. A study is also being performed for delaminations that can form near the matrix crack tip.

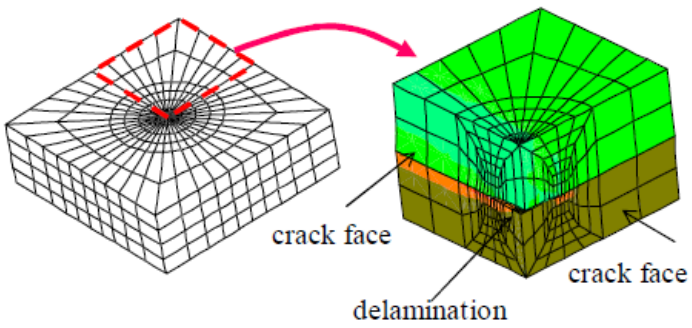

Fig. 19 Modeling of delamination at the intersection of cracks

The strain energy release rate for a delamination at the intersection of matrix cracks (Fig. 19) was calculated. Fig. 19 shows a finite element model with a circular delamination at the crossing matrix cracks. The strain energy release rate has been calculated for various stacking sequences for circular delaminations. Other delamination shapes, which are more realistic, will

be also studied in future work. The opening due to matrix cracks and the delamination at the crossing matrix cracks is currently being investigated. Finite element models were developed and analyzed under axial and biaxial loadings.

V. CONCLUSIONS

Optimal design of composite wind turbine blades requires an analysis that can predict microcracking under harsh environmental conditions. The current work is focused on laying the foundation for such an analysis. This requires experimental techniques to simulate the operating environment for the wind turbine, because this latter undergoes severe loading conditions. The high stress level can be reduced using insulating technique under low temperature, and the design method for lamina and laminate thickness should be considered.

In this chapter, transient thermomechanical finite element analysis was performed to study the effect of thermal shock for composite laminates with different material systems and lay-ups. Higher out-of-plane stresses on the free-edge were found in lay-up 1 for both material systems (IM7/977-2, IM7/5250-4). The IM7/5250-4 has higher out-of-plane stresses on the free-edge under thermal loading than the IM7/977-2 has. Both IM7/977-2 and IM7/5250-4 composite laminates have a peak point in the stress curve in a very short time; however, IM7/977-2 has higher out-of-plane stress at the peak point in the stress curve. The out-of-plane stress on surface ply is considered to be similar for both lay-ups. However, the stress pattern is quite different at very short time. The stress pattern is dramatically changed according to the stacking sequences for both materials, and this is the reason why study for lay-ups should be performed. The stacks starting with 0 ° fibre orientation have better stress pattern than stacks starting with other degrees, and the angle ply laminates have lower stress level than cross play laminates. Optimal design of composite blades requires an analysis that can predict microcracking induced permeability. The current work is focused on laying the foundation for such analysis. This requires the development of experimental techniques to simulate the operating environment for blades. Also, the study of thermal shock effect due to harsh environment needs to be investigated. Actual wind turbine composite blades do not have edges. However, coupon specimens, which are usually used for material testing due to the difficulty of full size testing, have edges. These free-edges could be the reason of edge delaminations during testing of composite laminates. This study examined the ply-level damage accumulated due to cycling IM7/977-2 and IM7/5250-4 cross-ply and angle-ply composite laminates under thermomechanical loadings.

No crack occurred up to 20 thermal cycles for 18-ply graphite epoxy IM7/977-2 laminates with $[0/-45/90/45/0/-45/90/45/0]_S$ stacking sequence. However, thermal cycling followed by the mechanical cycling (uniaxial tension loads) at room temperature, resulted in a rapid increase of microcracking induced damage. The highest rate of increase of damage densities was observed, when the specimen was mechanically cycled (uniaxial tension loads) at low temperatures. After uniaxial tension test at low temperature, delaminations were observed between the -45 ° and 90 ° plies (2nd and 3rd plies from outer surface) as well as 90 ° and 45 ° plies (3rd and 4th plies from outer surface). Delaminations at transverse crack tips were also observed, which could be more critical for the permeability and leakage problem.

No cracks occurred up to 500 cycles for four-point bending test at room temperature for 8-ply graphite epoxy IM7/5250-4 laminates with $[90_2/0_2]_S$ stacking sequence. However, four-point bending test at -196 ℃ resulted in transverse matrix cracks after 10 cycles on 90 degree ply (1st ply from outer surface). The parallel cracks to the specimen length direction for four-point bending test at room temperature were observed after 30 cycles on 90 ° ply. However, transverse matrix cracks were observed after four-point bending test at -196 ℃ on 90 ° ply. The length of cracks for four-point bending test at room temperature was between 12 μm and 50 μm after 30 cycles and increased up to 100 μm after 50 cycles. After 10 cycles for four-point bending test at -196 ℃, 250 μm of crack length was observed.

On applying thermal cycling to the specimen of 8-ply graphite epoxy IM7/5250-4 laminates with $[90_2/0_2]_S$ stacking sequence with wax insulation, the material showed no sign of crack development up to 40 cycles. However, cracks were initiated in the specimen without wax insulation after 33 thermal cycles on 90 ° ply (1st ply from outer surface).

REFERENCES

[1] B. Yang. and D. Sun, “Testing, inspecting and monitoring technologies for wind turbine blades: A survey,” Renewable and Sustainable Energy Reviews 22 (2013) 515-526.

[2] O. Parent and A. Ilinca, “Anti-icing and de-icing techniques for wind turbines: Critical review,” Cold Regions Science and Technology 65 (2011) 88-96.

[3] B. Natarajan et. al., Structural Analysis of Composite Wind Turbine Blade using Advanced Beam Model Approach, International Journal of Precision Engineering and Manufacturing, vol. 13, no. 12, 2245-2250, 2012.

[4] Bong Taek Oh, J. Noh, D. Lagoudas, and J. Whitcomb, Effect of Thermal Shock on Damage in Cryogenic Composite Laminates, 18th Annual Technical Conference American Society for Composites, Gainesville, Florida, Oct. 19-22 (2003).

[5] B. A. Boley and J. H. Weiner, “Theory of Thermal Stress” Dover Pub. Inc.

[6] Mohamed Elseifi, “A New Scheme for the Optimum Design of Stiffed Composite Panels with Geometric Imperfections,” Ph.D. Dissertation, College of Engineering, Virginia Polytechnic Institute and State University, 1998.

[7] Q. Li, L. Minnetyan, C. C. Chamis, “Structural Durability and Fatigue of Composites in Acoustic Environment,” Society for the Advancement of Materials and Process Engineering, Long Beach, CA, May 2002.

[8] S. Venkataraman, "Modeling, Analysis and Optimization of Cylindrical Stiffened Panels for Reusable Launch Vehicles Structures," Ph.D. Dissertation, College of Engineering, University of Florida, 1999.

[9] Robinson MJ et al. "Hydrogen permeability requirements and testing for reusable launch vehicle tanks," Proceedings of the 43rd AIAA/ASME/ASCE/AHS/ASC Structures, Structural Dynamics, and Materials Conference, Denver, CO; 2002. AIAA-2002-1418.

[10] S.S. Kessler, T. Matuszeski and H. McManus. "Cryocycling and Mechanical Testing of CFRP for the X-33 Liquid H_2 Fuel Tank Structure," Proceedings of the American Society for Composites (ASC), Sep. 9-12, 2001, Virginia Tech, Blacksburg.

[11] R. Y. Kim and S. L. Donaldson, Experimental Observation of Microcracking of Composite Laminates under Cryogenic Temperature, AIAA, Aug., 28-30 (2001).

[12] V. T. Bechel, M. B. Fredin, and S. L. Donaldson. "Combined Cryogenic and Elevated Temperature Cycling of Carbon/Polymer Composites," Society for the Advancement of Materials and Process Engineering, Long Beach, CA, May 2002.

[13] Bong Taek Oh, D. C. Lagoudas and S. Moon, Mechanical Characterization in laminated composite for cryogenic application, Polymer Composites, vol. 34, iss. 5, 607-615, May 2013.

[14] Bong Taek Oh, D. C. Lagoudas and S. Moon, Effect of insulation layer for thermal shock in cryogenic composite laminates, Polymer Composites, vol. 34, iss. 4, 531-536, Apr. 2013.

Oh Bong Taek is the CEO of TOMS (Technology of Material Science) Co., LTD. and the adjunct professor of Mechanical Design Engineering at Chung Nam National University. The primary research areas of interest include structural stress analysis, composite design/analysis/test/repairing, and also CNT composites.

Dr. Oh received the Bachelor and M.S. of mechanical engineering degree from SoongSil University, Korea, and Doctorate degree (D.En.) in aerospace engineering from Texas A&M University in U.S.A.

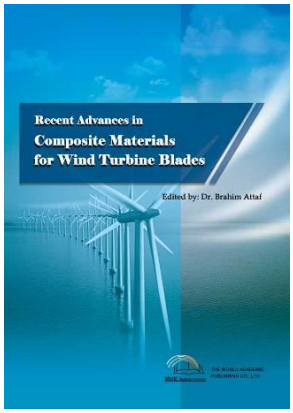

Recent Advances in Composite Materials for Wind Turbine Blades
Edited by Dr. Brahim Attaf

ISBN 978-0-9889190-0-6

Hard cover, 232 pages

Publisher: The World Academic Publishing Co. Ltd.

Published in printed edition: 20, December 2013

Published online: 20, December 2013

This book of science and technology provides an overview of recent research activities on the application of fibre-reinforced composite materials used in wind turbine blades. Great emphasis was given to the work of scientists, researchers and industrialists who are active in the field and to the latest developments achieved in new materials, manufacturing processes, architectures, aerodynamics, optimum design, testing techniques, etc.. These innovative topics will open up great perspectives for the development of large scale blades for on- and off-shore applications. In addition, the variety of the presented chapters will offer readers access to global studies of research & innovation, technology transfer and dissemination of results and will respond effectively to issues related to improving the energy efficiency strategy for 2020 and the longer term.

How to cite this book chapter

Bong Taek Oh (2013). Study of Composite and Sandwich Plates Extracted from Wind Turbine Blade Structures under Harsh Environmental Conditions, *Recent Advances in Composite Materials for Wind Turbines Blades*, Dr. Brahim Attaf (Ed.), ISBN 978-0-9889190-0-6, WAP-AMSA, Available from: http://www.academicpub.org/amsa/chapterInfo.aspx

World Academic Publishing - Advances in Materials Science and Applications